COBEM 2023 27TH INTERNATIONAL CONGRESS OF MECHANICAL ENGINEERING

ABCM Brazilian Society of Mechanical Sciences and Engineering
27th ABCM International Congress of Mechanical Engineering
December 04-08, 2023, Florianópolis-SC, Brazil

COB-2023-1476
Numerical simulation of flow and pollutant dispersion in an urban intersection using k-ϵ turbulence model

Tomaz Antônio Lisboa e Silva
Fernanda Capucho Cezana
Federal Institute of Science and Technology of Espírito Santo - *campus* São Mateus
tmz.lisboa@hotmail.com
fecezana@ifes.edu.br

Abstract. *The dispersion of pollutants in urban intersections is a complex problem that can be influenced by a series of factors, such as building geometry, wind direction, traffic density, and the location of pollution sources. Traffic density can significantly affect pollutant dispersion, and it is directly affected by the number of cars present in an urban area. This factor is important to understanding how to reduce pollutant concentrations. In this paper, the finite volume method together with a non-structured polyhedral mesh was used, in which it solved the mass, momentum and chemical species conservation equations, using the Ansys Fluent© 23.0 computational code, combined with the realizable k-ϵ turbulence closure model. The method's validation was carried out using the DAPPLE model-based boundary conditions, and the initial model comparisons and velocity profiles (without incorporating cars). This step was crucial to ensure the necessary reliability and relevance of both the quantitative and qualitative results. Following the successful validation of the method, the study proceeded to examine the impact of cars on the flow and dispersion of carbon monoxide at the intersection. This study utilizes a numerical simulation with a low computational cost, along with a high-performance mesh, and provides data for future research in the area, which can aid in making informed decisions about implementing pollution control measures. These measures may include adjusting traffic light timing and restricting vehicle traffic during peak hours. Furthermore, it is worth mentioning that this topic has a direct impact on the lives of people who live and work near these areas. Exposure to high levels of air pollution can lead to respiratory, cardiovascular, and neurological problems, among others. Therefore, it is crucial to improve the air quality of cities. To achieve this goal, the use of numerical approaches, such as computational fluid mechanics studies (for example, Reynolds-Averaged Navier-Stokes methods), is a valuable tool to aid urban planners make informed decisions on how to reduce air pollution in urban areas and protect public health.*

Keywords: *Pollutant Dispersion, Urban Intersection, Reynolds-Averaged Navier–Stokes, Computation Fluid Dynamics*

1. INTRODUCTION

The World Health Organization (WHO) has alarming estimates that 4 millions death occur each year worldwide due to preventable environment causes. Air pollution plays a significant role in these numbers, with nearly the entire global population (99%) being exposed to air pollution levels that exceed WHO's recommendations. Notably, studies conducted by Vardoulakis *et al.* (2003) revealed that the inhalation of high concentrations of carbon monoxide (CO) can result in a range of respiratory complications. It's important to address these pollutants adverse effects on human health and the environment.

Vehicular emissions play a major role in pollution of the air in large cities, highlighting the need for effective urban planning to combat this issue and improve air quality. Research conducted by Goulart *et al.* (2019) has revealed the substantial impact of building arrangements on atmospheric flow and pollutant dispersion. The study suggests that streets with a lower aspect ratio, which is determined by the quotient of the building height (h) and street width (W), are more conductive to effective pollutant dispersion.

In this context, Tiwary *et al.* (2011) offers valuable insights into the importance of intersection for urban planning. These regions are frequently associated with traffic congestion, leading to elevated levels of pollutants. The researchers emphasize that the airflow patterns within urban areas are significantly affected by the intersection's geometry, as well as the wind direction and velocity. Therefore, careful intersection planning plays a crucial role in optimizing traffic flow and ensuring efficient pollution mitigation.

The atmospheric flow is very complex and turbulent (Belcher, 2005) and it is associated with high Reynolds numbers. This implies the presence of numerous turbulent structures at small scales, which significantly increases the computational requirements. To address this challenge, researchers often employ the Reynolds Average Navier-Stokes (RANS) method.

The objective of this paper is to analyse numerically the flow and dispersion of carbon monoxide from standing vehicles in a real urban intersection using a Reynolds Averaged Navier-Stokes (RANS) methodology.

2. METHODOLOGY

2.1 Computational domain and mesh

This study utilizes Computational Fluid Dynamics (CFD) to simulate the flow and pollutant dispersion at an intersection located in Central London, between Marylebone Rd. and Gloucester Pl. The modeling approach involves mathematical and computational models to simulate fluid movement and pollutant dispersion in urban environments. Figure 1 shows the complete domain, which was used to validate the simplification (Figure 2) of the domain in order to improve simulation time, and the addition of cars as scalar sources. The complete domain was utilized to validate the experiment, although the specific validation details are not included in the paper. In Figure 1, the model's coordinates are marked in mm, with x_t from west to east, y_t from south to north, and z from ground to top, respectively. x, y, z are the computational coordinates.

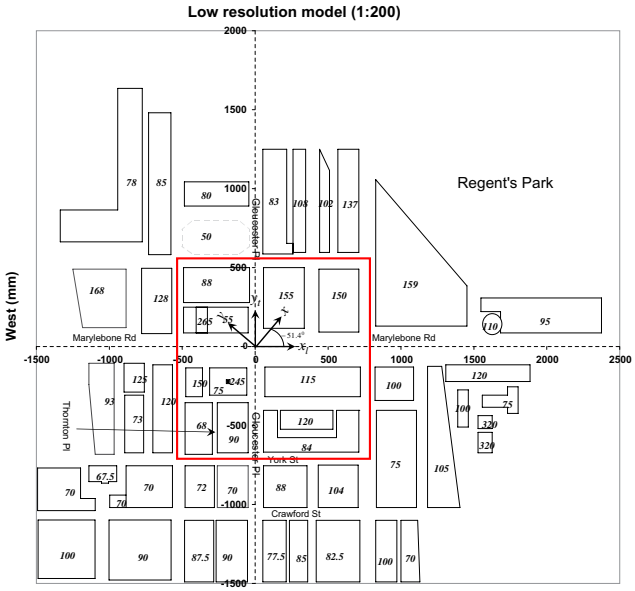

Figure 1: Plan view of the wind tunnel model. The italicized numbers in each building block indicate their height in mm. The red square represents the area used in the simplification presented of Figure 2. (Xie and Castro, 2009).

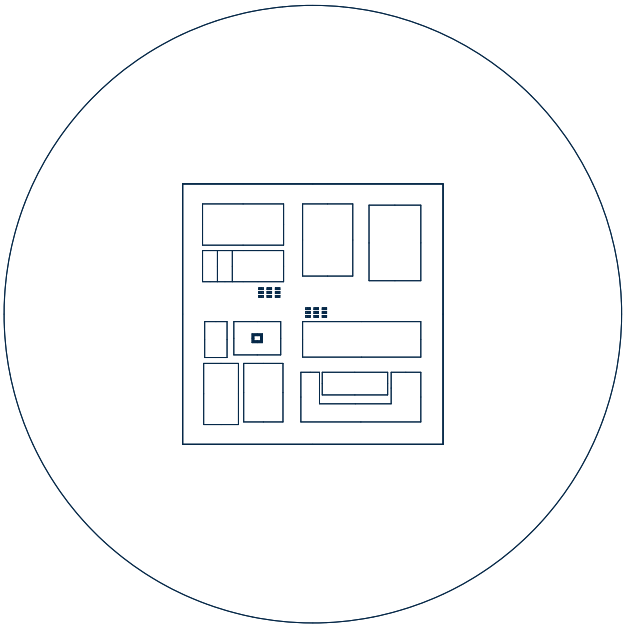

Figure 2: Adaptation performed in order to enhance the simulation's time.

Polyhedral mesh, as pointed out in Wang *et al.* (2021), is recognized for its superior precision, flexibility, wider

applicability, and overall better quality in comparison to tetrahedral meshes. To eliminate the need for mesh testing, in order to save time and resources, certain parameter were carefully selected (Table 1), such as low aspect ratio, high orthogonal quality, and low skewness, as recommended in Fluent (2009), although is recommended mesh testing to be sure of its influence, the method allows using the same mesh for all cases.

Property	**Current mesh**	**Reference Value**
Aspect Ratio	28.11	< 35
Skewness	0.69	< 0.95
Orthogonal Quality	0,3	> 0.1

Table 1: Mesh parameters

2.2 Governing equations and numerical methods

The fluid flow is characterized using mass and momentum conservation equations, represented by Eq. (1) and (2), respectively. Meanwhile, the dispersion of (CO) is described using Eq. (3), which follows an advective-diffusive transport equation. To account for turbulent effects, RANS is applied in all three equations, with the realizable $k-\epsilon$ model chosen as the turbulence model. Steady simulations were carried out with incompressible flow. In addition, neutral atmosphere was considered.

$$\frac{\partial \overline{u_j}}{\partial x_j} = 0; \tag{1}$$

$$\rho \frac{\partial \overline{u_i u_j}}{\partial x_j} = -\frac{\partial \overline{p}}{\partial x_i} + g\delta_{i3} + \mu \frac{\partial^2 \overline{u_i}}{\partial x_j \partial x_j} + \frac{\partial \tau_{ij}}{\partial x_j}; \tag{2}$$

$$\rho \frac{\partial \overline{u_i c}}{\partial x_j} = D \frac{\partial^2 \overline{c_i}}{\partial x_j \partial x_j} + M. \tag{3}$$

Where $\overline{u_i}$ and $\overline{p}$ represent mean velocity and mean pressure, respectively. $g\delta_{i3}$ is body force, τ_{ij} is defined as the Reynolds stress tensor, μ is dynamic viscosity, $\overline{c}$ represents mean concentration of scalar and M is the source term.

In this study, the realizable $k-\epsilon$ model was chosen, due to its ability to effectively model turbulent flows, including complex flow conditions. Shih *et al.* (1995a) emphasize the significance of this model, as it introduces reformulations in the turbulent model, particularly enhancing the transport equation for dissipation rate. These enhancements lead to improve accuracy and reliability in the obtained results. Eq. (4) and Eq. (5) describes the model.

$$\frac{\partial}{\partial x_j}(\rho k u_j) = \frac{\partial}{\partial x_j}\left[\left(\mu + \frac{\mu_t}{\sigma_k}\right)\frac{\partial k}{\partial x_j}\right] + G_b - \rho_\epsilon - Y_M + S_k \tag{4}$$

$$\frac{\partial}{\partial x_j}(\rho \epsilon u_j) = \frac{\partial}{\partial x_j}\left[\left(\mu + \frac{\mu_t}{\sigma_\epsilon}\right)\frac{\partial \epsilon}{\partial x_j}\right] + \rho C_1 S_\epsilon - \rho C_2 \frac{\epsilon^2}{k + \sqrt{\nu\epsilon}} + C_{1\epsilon}\frac{\epsilon}{k} + C_{3\epsilon} G_b + S_\epsilon \tag{5}$$

where,

$$C_1 = max\left[0.43, \frac{\eta}{\eta + 5}\right], \quad \eta = S\frac{k}{\epsilon}, \quad S = \sqrt{2 S_{ij} S_{ij}} \tag{6}$$

Where, ρ represents the fluid density, k denoting the turbulent kinetic energy and μ_t pertains to turbulent viscosity. The Prandtl number for turbulent kinetic energy is denoted as σ_k, and G_b represents the generation of turbulent kinetic energy due to buoyancy. Furthermore, ρ_ϵ accounts for the dissipation-induces destruction of turbulent kinetic energy, and Y_M signifies turbulent production resulting from mean shear. The term S_k corresponds to the source term associated with k, and ϵ characterizes the turbulent dissipation rate. The Prandtl number for turbulent dissipation rate is represented by σ_ϵ while S_ϵ refers to the user-defined source term linked with ϵ.

Equation 7 describe the turbulent behavior within the flow, and Eq. (8) introduces a new formulation for turbulent viscosity that incorporates realizability restriction. By enforcing these restrictions, the model outputs more reliable and credible results.

$$-\overline{u_i u_j} = \nu_\tau (U_{i,j} + U_{j,i}) - \frac{2}{3} k \delta ij \tag{7}$$

$$\nu_\tau = C_\mu \frac{k^2}{\epsilon} \tag{8}$$

The term $-\overline{u_i u_j}$ represents the Reynolds stress, δ_{ij} is the Kronecker delta, the parameter ν_τ represents the turbulent eddy viscosity. However, C_μ is not a constant on this model, and, as seen in Shih *et al.* (1995a), it is calculated by Eq. (9).

$$c_\mu = \frac{1}{A_0 + A_s U^{(*)} \frac{k}{\epsilon}} \tag{9}$$

Where A_0 is a constant coefficient, A_s is the shear factor, $U^{(*)}$ stands for turbulent velocity scale. For more details, see Shih *et al.* (1995b).

2.3 Description of numerical experiments and boundary conditions

The experiment aims to analyze the impact of wind direction. To achieve this, three conditions were simulated: $0°$, $90°$, and $51.4°$, bases on the complete geometry described in Xie and Castro (2009), although, those results are not shown here. The $0°$ represent a wind parallel to Marylebone Road, while the $90°$ direction corresponds to a wind parallel to Gloucester Place.

For the second step, the geometry was simplified, and obstacles in the shape of cars were inserted at the intersection. This enabled the creation of a mesh with improve quality, facilitated analysis of their influence on the flow.

The reference velocity is given by the Reynold's equation:

$$Re = \frac{\rho \cdot U_{ref} \cdot h_m}{\mu} \quad \therefore \quad U_{ref} = \frac{Re \cdot \mu}{\rho \cdot h_m} \tag{10}$$

Were $Re = 18 \cdot 10^3$ represents the Reynold's number, and is recommended at Xie and Castro (2009), it was kept constant, $h_m = 27.8\,m$ represent the mean height of the buildings on the simplified geometry, $\rho = 1.225\,kg/m^3$ is air density, μ represents the dynamic viscosity, and it results on a $U_{ref} = 1.89\,m/s$m. The dimensionless profile can be seen at Xie and Castro (2009).

The method employed eliminates the need to set up and outlet condition, as the outermost boundary is designated as an in inlet. This ensures that the flow is directed inward across the entire surface of the cylinder, effectively functioning as an outflow when the velocity vector points outward. Consequently, these boundaries do not interfere with the flow in the areas of interest. The adopted diffusion coefficient ($C_{\mu_{eff}}$) set at $\mu_{eff}/1$, where, μ_{eff} represents the effective viscosity relative to the Schmidt number. The scalar source term was defined as shown in Eq. (11).

$$S = \frac{U_{ref} \cdot h_m^2 \cdot \mu}{\forall} \tag{11}$$

On this equation, $\forall$ signifies the volume of an individual cell, strategically positioned behind of each vehicle to represent the CO emission effects. Only in these specific cells the source term is taken into account.

Buildings, cars and the floor are treated as a no-slip condition, indicating that the fluid's velocity field is equal to zero at these boundaries. In addition, the mass flux of the scalar is also considered to be zero in these regions. On the other hand, on the top of the domain was set as a free-slip condition and the mass flux of scalar is considered as zero.

3. RESULTS AND DISCUSSION

3.1 Flow characteristics at the intersection and the influence of cars

The presence of a car has various effects on the surrounding airflow. According to Carpentieri *et al.* (2012), the airflow around the vehicle can be divided into two distinct regions: the near wake and the far wake. In the near wake, which forms immediately behind the vehicles, there is a significant region of air recirculation. Additionally, there are longitudinal drag vortices, causing areas of unstable and fluctuating airflow. There, vortices result from different factor, such as instability of the air layer separating from the vehicle and the movement of air in the wake region.

In order to comprehend the alterations in air flow induced by a moving vehicle, the E&H model proposed by Eskridge and Hunt (1979) plays a pivotal role. this theoretical model approach offers valuable insights into the gradual reduction in air velocity as we distance ourselves from the vehicle and enter the far wake region. By integrating crucial factors such as vehicle's velocity, geometry, and atmospheric conditions, the E&H model offers an effective means to estimate and explore the intricate airflow dynamics in this specific area.

In this paper, was assumed stationary vehicles with a relative air velocity. Examining Figure 3 it becomes clear that the wind direction has a significantly greater influence on the flow pattern than the presence of vehicles.

The selected height of $8 \cdot 10^{-3}\,m$ is equivalent to the height of an average person, approximately $1,6\,m$. This decision was based on the fact that this height is commonly observed in teenagers, and many individuals generally fall within this height range. This decision was mas made while employing a scale of 1:200.

Figure 4 illustrates the quantitative representation of how wind direction affects flow at the intersection, taking obstacles into account. Notably, even with the presence of vehicles, there are similarities in the flow pattern without any cars (not shown). However, it is important to emphasize that the predominant influence in this context is the wind direction, even in low wind speed conditions.

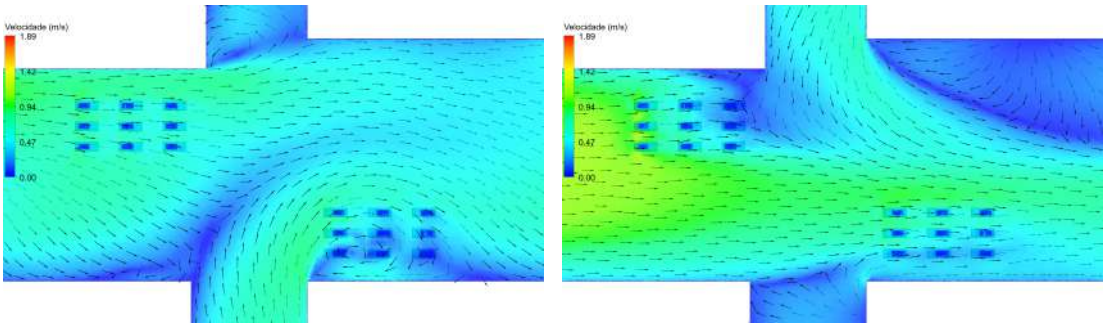

(a) 51.4°

(b) 0°

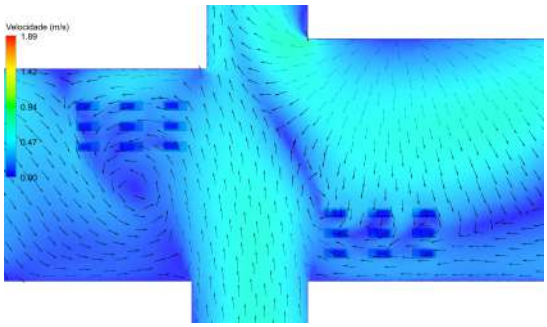

(c) 90°

Figure 3: Flow profile at the intersection with the car at $z = 8 \cdot 10^{-3}\, m$.

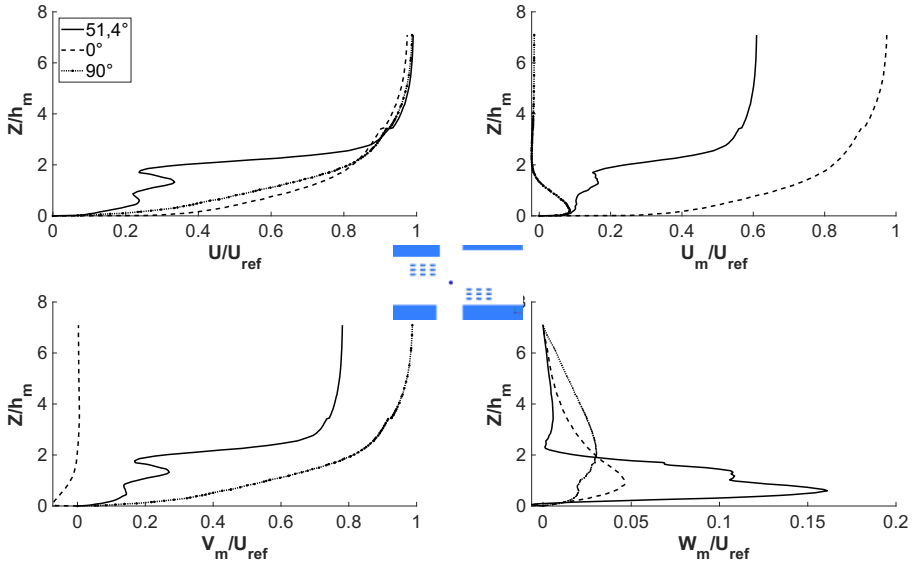

Figure 4: Comparison of velocity profiles for different wind directions in simulations using the simplified geometry, at the center of the intersection between Marylebone Rd. and Gloucester Pl.

The orientation of the external wind with respect to the intersection holds a significant influence over pollutant dispersion. When examining diagonal wind direction (Figure 5) in relation to the street axis, the results of pollutant dispersion demonstrate reasonable agreement with the experiments conducted by Soulhac *et al.* (2009).

These observations suggest that the wind direction can influence how pollutants disperse at the intersection. As a result, there are notable variations in the distribution and concentration of pollutants in different streets.

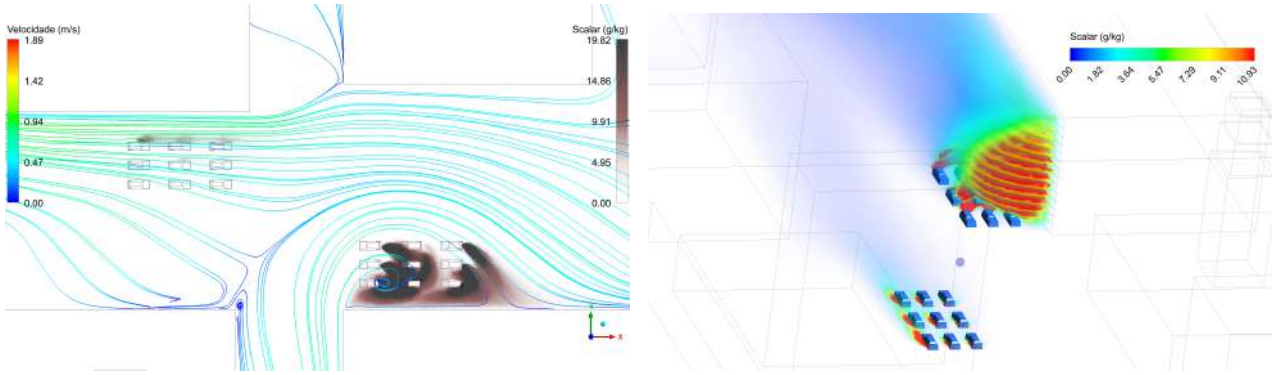

(a) Streamlines and scalar concentration. (b) Scalar plume

Figure 5: Scalar plume at the intersection of Marylebone Rd. and Gloucester Pl. at $z = 8 \cdot 10^{-3}\, m$ for $51.4°$ (diagonal direction).

Figure 7 serves as a valuable complement to Figure 6, revealing how wind direction directly affects scalar concentration at the intersection. When the flow aligns parallel to Gloucester Pl. a peak of concentration appears near the main intersection. Along the street the concentration is near zero. This is physically consistent, as the main direction of the flow is parallel to Gloucester Pl., so along Marylebone Rd. the concentration values will be very small (except at the principal intersection). On the other hand, when the flow is parallel to Marylebone Rd. the dispersion of pollutants is favored because the flow is channeled, carrying the pollutants out of the domain. In addition, the peak concentration is located after the main intersection. In the case of wind direction of 51.4°, the concentration values are very small. This shows that, for this wind direction, the pollutants will disperse more easily throughout the region and out of the domain.

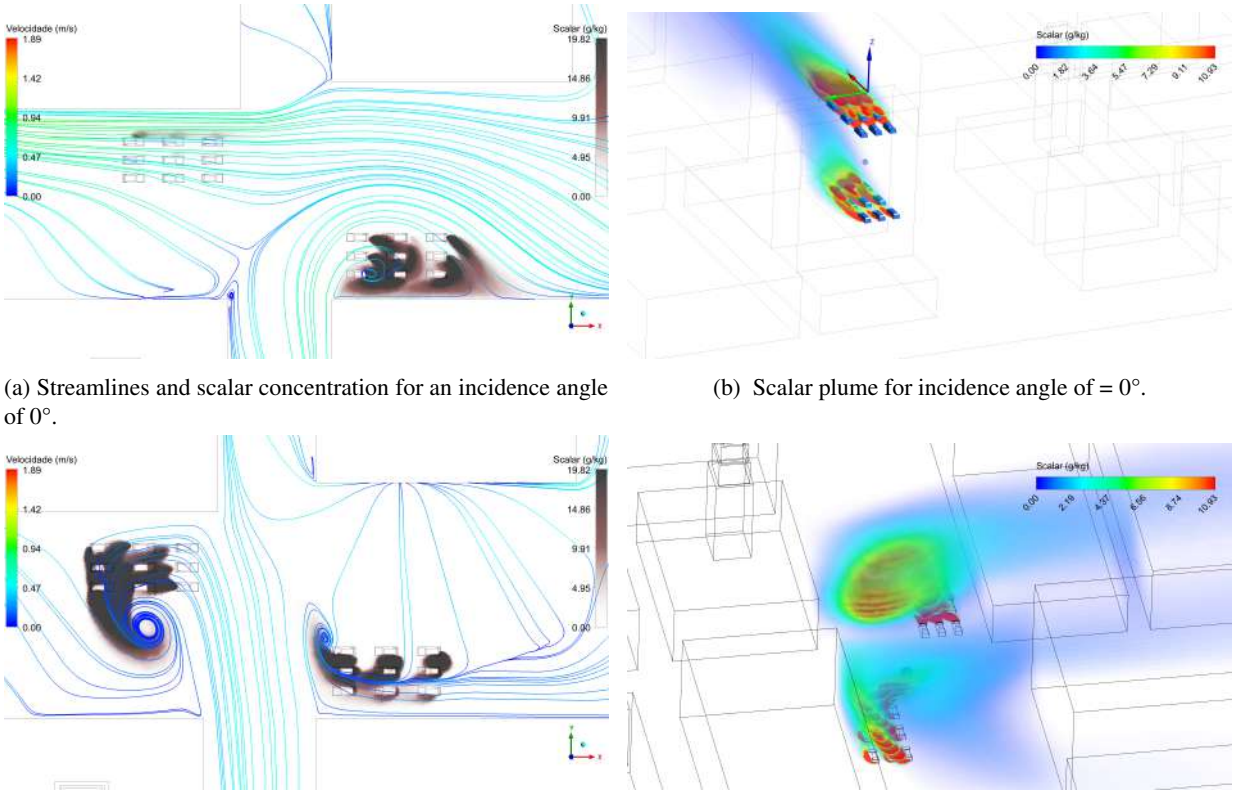

(a) Streamlines and scalar concentration for an incidence angle of 0°.

(b) Scalar plume for incidence angle of = 0°.

(c) Streamlines and scalar concentration for an incidence angle of 90°.

(d) Scalar plume for incidence angle of = 90°.

Figure 6: Scalar plume at the intersection of Marylebone Rd. and Gloucester Pl. at $z = 8 \cdot 10^{-3}\, m$, for winds parallel to the streets.

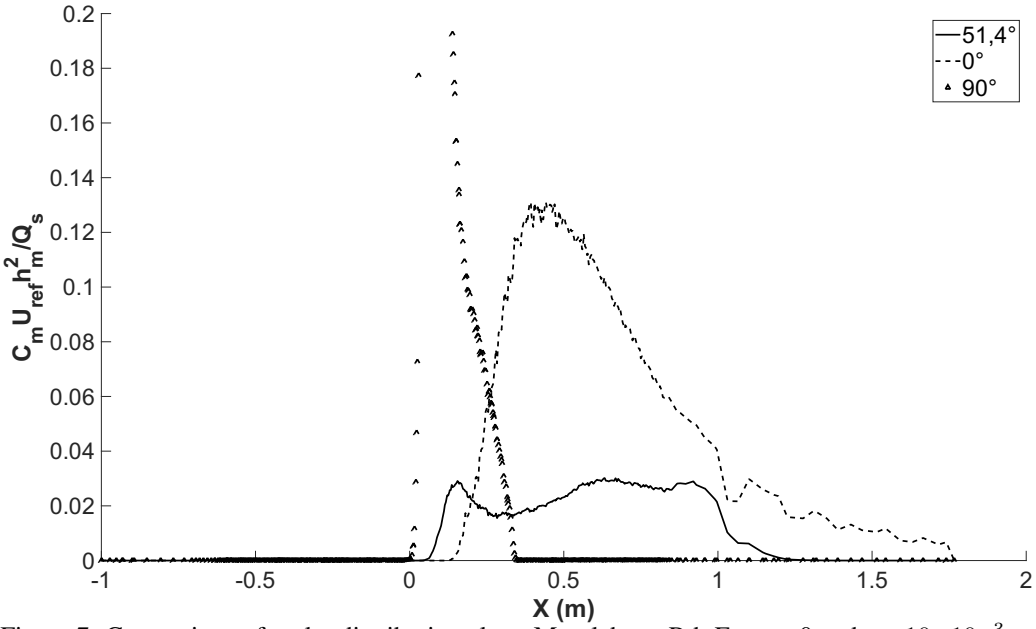

Figure 7: Comparison of scalar distribution along Marylebone Rd. For y = 0 and z = $10 \cdot 10^{-3} m$.

4. Conclusion

The RANS model proved valuable for studying pollutant dispersion at an intersection. It offered importants qualitative insights into flow patterns and pollutant dispersion. In quantitative analysis, it performed well neat pollutant sources but had limitations for long-distance transport.

Wind direction emerged as a critical factor significantly influencing pollutant dispersion. Perpendicular winds were associated with higher pollutant concentrations, while parallel winds showed efficient pollutant dispersion. Winds at $51.4°$ exhibited an intermediate behaviour, with higher concentrations found only in certain corners.

The simplified domain effectively captured essential flow characteristics, even with the inclusion of cars as pollutant sources. Cars had a substantial impact on pollutant concentration, consistent with simulations using the complete geometry.

Considering these findings, analysing pollutant dispersion requires accounting for flow characteristics, environmental conditions, and source distribution to ensure more comprehensive assessments.

5. REFERENCES

Belcher, S., 2005. "Mixing and transport in urban areas". *Philosophical Transactions of the Royal Society A: Mathematical, Physical and Engineering Sciences*, Vol. 363, No. 1837, pp. 2947–2968. doi:10.1098/rsta.2005.1673.

Carpentieri, M., Kumar, P. and Robins, A., 2012. "Wind tunnel measurements for dispersion modelling of vehicle wakes". *Atmospheric Environment*, Vol. 62, pp. 9–25. ISSN 1352-2310. doi:https://doi.org/10.1016/j.atmosenv.2012.08.019. URL `https://www.sciencedirect.com/science/article/pii/S1352231012007911`.

Eskridge, R.E. and Hunt, J., 1979. "Highway modeling. part i: prediction of velocity and turbulence fields in the wake of vehicles". *Journal of Applied Meteorology and Climatology*, Vol. 18, No. 4, pp. 387–400.

Fluent, 2009. *ANSYS FLUENT 12.0/12.1 Documentation*. Ansys Inc.

Goulart, E., Reis, N., Lavor, V., Castro, I., Santos, J. and Xie, Z., 2019. "Local and non-local effects of building arrangements on pollutant fluxes within the urban canopy". *Building and Environment*, Vol. 147, pp. 23–34. ISSN 0360-1323. doi:https://doi.org/10.1016/j.buildenv.2018.09.023. URL `https://www.sciencedirect.com/science/article/pii/S0360132318305717`.

Shih, T.H., Liou, W.W., Shabbir, A., Yang, Z. and Zhu, J., 1995a. "A new k-ϵ eddy viscosity model for high reynolds number turbulent flows". *Computers Fluids*, Vol. 24, No. 3, pp. 227–238. ISSN 0045-7930. doi:https://doi.org/10.1016/0045-7930(94)00032-T. URL `https://www.sciencedirect.com/science/article/pii/004579309400032T`.

Shih, T.H., Zhu, J. and Lumley, J.L., 1995b. "A new reynolds stress algebraic equation model". *Computer Methods in Applied Mechanics and Engineering*, Vol. 125, No. 1, pp. 287–302. ISSN 0045-7825. doi:https://doi.org/10.1016/0045-7825(95)00796-4. URL `https://www.sciencedirect.com/science/article/pii/0045782595007964`.

Soulhac, L., Garbero, V., Salizzoni, P., Mejean, P. and Perkins, R., 2009. "Flow and dispersion in street intersections". *Atmospheric Environment*, Vol. 43, No. 18, pp. 2981–

2996. ISSN 1352-2310. doi:https://doi.org/10.1016/j.atmosenv.2009.02.061. URL https://www.sciencedirect.com/science/article/pii/S1352231009001186.

Tiwary, A., Robins, A., Namdeo, A. and Bell, M., 2011. "Air flow and concentration fields at urban road intersections for improved understanding of personal exposure". *Environment International*, Vol. 37, No. 5, pp. 1005–1018. ISSN 0160-4120. doi:https://doi.org/10.1016/j.envint.2011.02.006. URL https://www.sciencedirect.com/science/article/pii/S0160412011000377.

Vardoulakis, S., Fisher, B.E., Pericleous, K. and Gonzalez-Flesca, N., 2003. "Modelling air quality in street canyons: a review". *Atmospheric Environment*, Vol. 37, No. 2, pp. 155–182. ISSN 1352-2310. doi:https://doi.org/10.1016/S1352-2310(02)00857-9. URL https://www.sciencedirect.com/science/article/pii/S1352231002008579.

Wang, W., Cao, Y. and Okaze, T., 2021. "Comparison of hexahedral, tetrahedral and polyhedral cells for reproducing the wind field around an isolated building by les". *Building and Environment*, Vol. 195, p. 107717. ISSN 0360-1323. doi:https://doi.org/10.1016/j.buildenv.2021.107717. URL https://www.sciencedirect.com/science/article/pii/S0360132321001281.

WHO, W.H.O., 2022. "Billions of people still breathe unhealthy air: new who data". Https://www.who.int/news/item/04-04-2022-billions-of-people-still-breathe-unhealthy-air-new-who-data.

Xie, Z.T. and Castro, I.P., 2009. "Large-eddy simulation for flow and dispersion in urban streets". *Atmospheric Environment*, Vol. 43, No. 13, pp. 2174–2185. ISSN 1352-2310. doi:https://doi.org/10.1016/j.atmosenv.2009.01.016. URL https://www.sciencedirect.com/science/article/pii/S135223100900034X.

6. RESPONSIBILITY NOTICE

The authors are solely responsible for the printed material included in this paper.